Supporting Information for "Toward Practical Quantum Embedding Simulation of Realistic Chemical Systems on Near-term Quantum Computers"

Weitang Li,[1,2] Zigeng Huang,[1] Changsu Cao,[1] Yifei Huang,[1] Zhigang Shuai,[2] Xiaoming Sun,[3,4] Jinzhao Sun,[5] Xiao Yuan,[6] and Dingshun Lv[1,*]

[1] *ByteDance Inc, Zhonghang Plaza, No. 43, North 3rd Ring West Road, Haidian District, Beijing.*

[2] *Department of Chemistry, Tsinghua University, Beijing 100084, China*

[3] *Institute of Computing Technology, Chinese Academy of Sciences*

[4] *University of Chinese Academy of Sciences*

[5] *Clarendon Laboratory, University of Oxford, Oxford OX1 3PU, UK*

[6] *Center on Frontiers of Computing Studies, Peking University, Beijing 100871, China*

I. METHODS

In this section, we will first review the basics of the quantum embedding methods, following the discussions in previous works [1–3]. We then introduce the our methods DMET-ESVQE in Section I B. We further discuss the practical implementation for molecular systems.

A. Review of density matrix embedding theory

Density matrix embedding is one of the representative methods in the quantum embedding theory, first proposed in 2012 [2, 3], which converts the original quantum system into a system composed of a fragment, the corresponding bath, and the pure environment. The basic idea is to compress the dimension of the system by Schmidt decomposition of the wave function. Imagine a Hilbert space composed of two orthonormal subspaces called fragment A with dimension L_A and environment B with dimension L_B ($L_A < L_B$). the dimension of any wave function $|\Psi\rangle$ in this Hilbert space can be decomposed by Schmidt decomposition as

$$|\Psi\rangle = \sum_{i}^{L_{\mathrm{A}}} \sum_{j}^{L_{\mathrm{B}}} \Psi_{ij} |A_i\rangle |B_j\rangle = \sum_{i}^{L_A} \sum_{j}^{L_B} \sum_{\alpha}^{L_A} U_{i\alpha} \lambda_\alpha V^\dagger_{\alpha j} |A_i\rangle |B_j\rangle = \sum_{\alpha}^{L_A} \lambda_\alpha |\tilde{A}_\alpha\rangle |\tilde{B}_\alpha\rangle, \tag{1}$$

where the states $|\tilde{B}_\alpha\rangle = \sum_j^{L_B} V^\dagger_{\alpha j} |B_j\rangle$ are defined as the bath orbitals which are entangled with fragment orbitals $|\tilde{A}_\alpha\rangle = \sum_i^{L_{\mathrm{A}}} U_{i\alpha} |A_i\rangle$. If $|\Psi\rangle$ is the ground state of a Hamiltonian H, then it must also be the ground state of

$$\hat{H}_{\mathrm{emb}} = \hat{P} \hat{H} \hat{P}, \tag{2}$$

which is the Hamiltonian for the embedded system composed of fragment plus its bath with the projector defined by

$$\hat{P} = \sum_{\alpha\beta} |\tilde{A}_\alpha \tilde{B}_\beta\rangle \langle \tilde{A}_\alpha \tilde{B}_\beta|. \tag{3}$$

The spirit of DMET is that the solution of a small embedded system is the exact equivalent to the solution of the full system [1], while the dimensions could be greatly reduced. However,

* lvdingshun@bytedance.com

the construction of $\hat{P}$ requires the exact ground state of the full system $|\Psi\rangle$ and thus the introduction of approximations is necessary. In practice, DMET algorithm is designed in a bootstrap manner. The mean-field approximation will be used for the full system to carry out the Schmidt decomposition and the embedded system will be solved by high-level method. Some constraints will be introduced to regulate the high-level results for further improvement.

B. Procedure of DMET-ESVQE

The entire process of calculating a chemical system by DMET-ESVQE is outlined as follows.

1. Partition the system into several fragments. Perform low-level, mean-field calculation on the entire system to obtain the ground state $|\Phi_0\rangle$.

2. Select a fragment from the system, construct the corresponding bath from $|\Phi_0\rangle$ by Schmidt decomposition. Construct the projector $\hat{P}$ and then obtain $\hat{H}_{\text{emb}} = \hat{P}\hat{H}\hat{P}$ for the embedded system.

3. Calculate the one-body (^1D) and two-body reduced density matrix (^2D) of the embedded system by ESVQE simulated on a classical computer or real quantum device in the future. Check if all the fragments have been traversed. If not, go back to step 2 and move to the next fragment.

4. Check if the constraint has been satisfied. The different limitation has a different cost function CF (see details in Section I C). For the single-shot DMET, the global chemical potential μ_{global} is introduced to conserve the electron number. If $\mathcal{L}(\mu_{\text{global}})$ is more than a settled threshold τ, go back to step 3 with the optimized μ_{global}, and re-calculate all the fragments.

5. Calculate expectations such as the total energy of the system democratically.

The pseudocode of the above DMET workflow is outlined in Algorithm 1.

Algorithm 1: Pseudocode for Density Matrix Embedding Theory

Partition the full system with a given scheme ;
$|\Phi_0\rangle \leftarrow$ low-level method ;
$\mu_{\text{global}} \leftarrow 0$;
$\tau \leftarrow 10^{-5}$;
do
  for fragment $A \in$ system **do**
    Construct bath orbitals, $|B_q\rangle \leftarrow |\Phi_0\rangle, |A_p\rangle$;
    Build projection matrix, $\hat{P} \leftarrow |A_p\rangle, |B_q\rangle$;
    Obtain embedding Hamiltonian, $\hat{H}_{\text{emb}} \leftarrow \hat{H}, \hat{P}, \mu_{\text{global}}$;
    Get ${}^1D_A$ and ${}^2D_A$ by ESVQE, ${}^1D_A, {}^2D_A \leftarrow \hat{H}_{\text{emb}}, |A_p\rangle, |B_q\rangle$;
  end
  CF(μ_{global}) and $\mu_{\text{global}} \leftarrow N_{\text{occ}}, \sum_A {}^1D_A$;
while $|\text{CF}(\mu_{\text{global}})| > \tau$;
Calculate observable expectation of interest $\leftarrow \sum_A {}^1D_A, \sum_A {}^2D_A$

In the following, we discuss the construction of the embedding Hamiltonian in Section I C, the constraints in the practical implementation for realistic quantum chemistry problems in Section I D and the implementation details of ESVQE in I E.

C. Construction of embedded system in interaction formulation

In this subsection, we discuss the strategy proposed in Ref. [1]. A straightforward approximation for the exact ground state is the low-level Hartree-Fock wave function. DMET uses this low-level wave function to construct the bath orbitals and solve the embedded system with a high-level solver. The low-level wave function $|\Phi_0\rangle$ obtained from the mean-field method could be written in second quantization as follows:

$$|\Phi_0\rangle = \prod_{\mu \in N_{\text{occ}}} \hat{a}_\mu^\dagger |\text{vac}\rangle, \tag{4}$$

where $\{\hat{a}_k, \hat{a}_k^\dagger | k \leq L\}$ is the set of the annihilation and creation operators on L spin orbitals denoted by indices k, l. N_{occ} electrons are supposed to occupy the N_{occ} lowest spin orbitals denoted by index μ, ν. The mean-field state $|\Phi_0\rangle$ is obtained under a selected basis set, of which the annihilation and creation operators are $\{\hat{c}_k^\dagger, \hat{c}_k | k \leq L]\}$. For convenience,

all basis have been orthonormalized and localized. In this work, we use the meta-löwdin method implemented in PySCF for this purpose [4, 5], although other methods such as intrinsic atomic orbitals have been reported in the literature [3, 6]. $\{\hat{a}_\mu^\dagger, \hat{a}_\mu | \mu \leq N_{\text{occ}}\}$ and $\{\hat{c}_k^\dagger, \hat{c}_k | k \leq L\}$ are connected through a coefficient matrix C:

$$\hat{a}_\mu^\dagger = \sum_{k=1}^{L} \hat{c}_k^\dagger C_{k\mu}, \tag{5}$$

with the size of $L \times N_{\text{occ}}$. The one-body density matrix ${}^1D_{\text{mf}}$ of the state is obtained as

$${}^1D_{\text{mf},kl} = \langle \Phi_0 | \hat{a}_l^\dagger \hat{a}_k | \Phi_0 \rangle = \sum_{\mu}^{N_{\text{occ}}} C_{k\mu} C_{\mu l}^\dagger. \tag{6}$$

For convenience, it is assumed that the orbitals of a selected fragment A are constructed by the first L_A spin orbitals. The ${}^1D_{\text{mf}}$ could be written as

$${}^1D_{\text{mf}} = \begin{bmatrix} {}^1D^A_{(L_A \times L_A)} & {}^1D^{\text{inter}}_{(L_A \times (L-L_A))} \\ {}^1D^{\dagger\ \text{inter}}_{((L-L_A) \times L_A)} & {}^1D^B_{((L-L_A) \times (L-L_A))} \end{bmatrix}, \tag{7}$$

The environment submatrix ${}^1D^B_{\text{mf}}$ constructed from ${}^1D_{\text{mf}}$ can be decomposed as:

$${}^1D^B_{\text{mf}} = \sum_{q}^{L-L_A} \lambda_q^2 |B_q\rangle\langle B_q|, \tag{8}$$

where λ_q is the eigenvalue of the environment orbitals $|B_q\rangle$. The bath orbitals entangled with the fragment will contribute all the eigenvalues between 0 and 1 (or 2 if using spatial orbital), while occupied (1 or 2) and unoccupied (0) environment orbitals are separated from the embedded system, where the occupied environment orbital is named core orbital either. Due to MacDonald's theorem [7], the bath orbitals will have the same dimension with the fragment. In the active space language, there are essentially $2L_A$ active orbitals and the role of the rest $L - 2L_A$ orbitals is to provide an effective potential $\hat{V}_{pq}^{\text{eff}}$ to the Hamiltonian of the fragment based on the mean-field one-body reduced density matrix ${}^1D^{\text{mf}}_{m,n}$

$$\hat{V}_{pq}^{\text{eff}} = \sum_{m,n} \left[{}^1D^{\text{mf}}_{m,n} \left([pq|mn] - [pn|mq] \right) \right] \hat{a}_p^\dagger \hat{a}_q, \tag{9}$$

where we have continued to use m, n, k, l as the indices for the original spin-orbitals of the molecule and p, q, r, s as the indices for the rotated spin-orbitals of the embedded system

following the main text. The summation of m, n runs over all unentangled orbitals including the inactive orbitals $\Omega^A_{\rm mf}$. The embedded Hamiltonian can now be written as

$$\hat{H}_{\rm emb} = E_{\rm nuc} + \sum_{p,q} \tilde{d}_{pq} \hat{a}^\dagger_p \hat{a}_q + \sum_{p,q,r,s} \frac{1}{2} \tilde{h}_{pqrs} \hat{a}^\dagger_p \hat{a}^\dagger_q \hat{a}_r \hat{a}_s, \tag{10}$$

with $\tilde{d}_{pq}$ defined as the transformed one-electron kinetic and Coulomb energy plus the effective potential of the unentangled electrons

$$\tilde{d}_{pq} = \sum_{k,l} T^\dagger_{pk} d_{kl} T_{lq} + \sum_{m,n} \left[{}^1D^{\rm mf}_{m,n} \left([pq|mn] - [pn|mq] \right) \right], \tag{11}$$

and $\tilde{h}_{pqrs}$ defined as the transformed two-electron Coulomb interaction

$$\tilde{h}_{pqrs} = \sum_{k,l,m,n} T^\dagger_{pk} T^\dagger_{ql} h_{klmn} T_{mr} T_{ns} \tag{12}$$

where the transformation matrix T is written as:

$$T = \begin{bmatrix} I_{(L_A \times L_A)} & 0_{(L_A \times L_A)} \\ 0_{((L-L_A)\times L_A)} & B_{((L-L_A)\times L_A)}. \end{bmatrix}. \tag{13}$$

and $B_{((L-L_A)\times L_A)}$ are the L_A bath orbitals entangled with the fragment.

Based on $\hat{H}_{\rm emb}$, the one-body reduced density matrix ${}^1D^A_{\rm high}$ for the embedded system:

$${}^1D^A_{\rm high} = \begin{bmatrix} {}^1D^{{\rm frag},A}_{(L_A \times L_A)} & {}^1D^{{\rm inter},A}_{(L_A \times L_A)} \\ {}^1D^{\dagger\ {\rm inter},A}_{(L_A \times L_A)} & {}^1D^{{\rm bath},A}_{(L_A \times L_A)} \end{bmatrix}, \tag{14}$$

is obtained by a high-level quantum solver mentioned in Section I E and so is the two-body reduced density matrix ${}^2D^A_{\rm high}$.

D. Constraint for high-level solution

After solving all fragments, some constraints could be introduced to regulate the high-level solutions self-consistently [1]. The electrons would be re-distributed between the fragment and bath during the DMET iteration, and as a result the number of electrons in the fragments may not sum up to the total number of electrons of the full system.

A global chemical potential $\mu_{\rm global}$ is introduced to fix this problem by modifying the $H_{\rm emb}$ as

$$\hat{H}_{\rm emb} \leftarrow \hat{H}_{\rm emb} - \mu_{\rm global} \sum_{r \in \Omega^A}^{L_A} \hat{a}^\dagger_r \hat{a}_r. \tag{15}$$

Here, we have defined $\Omega^A = \bigcup_j \Omega_j^A \setminus \Omega_{\mathrm{mf}}^A$, where Ω_{mf}^A is a set of inactive orbitals treated at mean-field level and excluded from the DMET iteration. We note Ω_{mf}^A could be an empty set. The wavefunction in the fragment A can be represented by

$$|\Psi^A\rangle = |\Psi_{\Omega^A}\rangle \otimes |\Phi_{\mathrm{mf}}^A\rangle\,, \tag{16}$$

where $|\Psi_{\Omega^A}\rangle$ denotes the high-level wavefunction in the selected basis set Ω^A, and $|\Phi_{\mathrm{mf}}^A\rangle$ is the mean-field solution, a single product state spanning the basis of inactive orbital Ω_{mf}^A. The role of Φ_{mf}^A is providing an effective potential $\hat{V}_{pq}^{\mathrm{eff}}$ to the embedded Hamiltonian via Eq 9. We can find that ${}^1D_{rr}^{\mathrm{mf}}$ is irrelevant to the self-consistency condition for single-shot DMET. Therefore, this method is different from those simply adopting an active space high-level solver, in which the inactive orbitals will be involved in the optimization process. In our workflow, the Newton-Raphson method has been used to optimize μ_{global} by solving the equation $\mathcal{L}\left(\mu_{\mathrm{global}}\right) = 0$.

As indicated in the main text, the single-shot DMET cost function is written as

$$\mathcal{L}\left(\mu_{\mathrm{global}}\right) = \left(\sum_A \sum_{r\in\Omega^A}^{L_A} {}^1D_{rr}^{\mathrm{frag},A}\left(\mu_{\mathrm{global}}\right) + N_{\mathrm{mf}} - N_{\mathrm{occ}}\right)^2, \tag{17}$$

where $N_{\mathrm{mf}} = \sum_A \sum_{r\in\Omega_{\mathrm{mf}}^A} {}^1D_{rr}^{\mathrm{mf}}$ is the number of electrons in the inactive orbitals obtained at mean-field level andN_{occ} is the total number of electrons. The solution could be improved further by eliminating the discrepancy between the mean-field one-body density matrix and the fragment one-body density matrix by adding a correlation potential $\hat{C}(u)$ to Hamiltonian $\hat{H}$:

$$\hat{H} \leftarrow \hat{H} + \hat{C}(u), \tag{18}$$

where $\hat{C}(u)$ takes the form

$$\hat{C}(u) = \sum_A \sum_{rs\in\Omega^A} u_{rs}\hat{a}_r^\dagger \hat{a}_s. \tag{19}$$

With inactive orbitals, the cost function can be written as

$$\mathcal{L}(u) = \sum_A \sum_{rs\in\Omega^A} \left({}^1D_{rs}^{\mathrm{frag},A} - {}^1D_{rs}^{\mathrm{mf}}(u)\right)^2 + \gamma \sum_{rs\in\bigcup_A \Omega_{\mathrm{mf}}^A} \left({}^1D_{rs}^{\mathrm{mf}}(u) - {}^1D_{rs}^{\mathrm{mf}}(0)\right)^2, \tag{20}$$

where ${}^1D_{rs}^{\mathrm{mf}}(0)$ is the one-body reduced density matrix without the fitted correlation potential and γ is a predefined weight constant. The last term ensures minimal effect of the correlation potential on the inactive orbitals Ω_{mf}^A.

The approach which only keeps the conservation of electron number is named as single-shot DMET [1], while the one that introduces the correlation potential is named as correlation potential fitting DMET (or self-consistent DMET) [1–3].

Single-shot DMET could also be modified case by case to improve the DMET performance or save the computational cost. In some cases, we are only interested in a small region in the whole system, such as the reaction center of a large organic molecule. Then the interested region can be treated as the only fragment and the calculation of the embedded system is carried out without any constraint. This modification is named active space DMET or DMET(AS) [1]. We note that from a chemical perspective, if FCI is used as the DMET solver, this exactly corresponds to a CASCI calculation and the role of DMET is to define an active space.

E. VQE with Energy Sorting Unitary Coupled Cluster Ansatz

In this work, we use the energy sorting strategy to construct a compact quantum circuit for the ground state searching. The workflow of ESVQE is summarized below:

1. Generate the reference state, i.e. the Hartree-Fock state, and construct the operator pool $\mathcal{O}$ to build the wave function ansatz. For UCCSD ansatz, the operator pool $\mathcal{O}$ consists of all the possible single- and double-excitation operators $\hat{T}_{pr}$ and $\hat{T}_{pqrs}$.

2. VQE optimization iteration is carried out for each operator $\hat{T}_i \in \mathcal{O}$ for E_i. The importance of the operator is evaluated by the energy difference with the reference state $\Delta E_i = E_i - E_{\text{ref}}$. $\Delta E_i = E_i - E_{\text{ref}}$ with $E_i = \min_{\theta_i} \langle \Psi_{\text{ref}} | e^{-\theta_i(\hat{T}_i - \hat{T}_i^\dagger)} \hat{H} e^{\theta_i(\hat{T}_i - \hat{T}_i^\dagger)} | \Psi_{\text{ref}} \rangle$ and $E_{\text{ref}} = \langle \Psi_{\text{ref}} | \hat{H} | \Psi_{\text{ref}} \rangle$ Then, sorted list $\mathcal{E} = \{(\Delta E_i, \hat{T}_i)\}_{\text{sorted}}$ is formed.

3. The operators with contributions above a threshold $|\Delta E_i| > \varepsilon$ are picked out and used to perform the VQE optimization. In this work we set $\varepsilon = 1 \times 10^{-5}$.

4. Finally, output the circuit parameters corresponding to the optimized wave function $|\Psi^{\text{opt}}\rangle$ together with the energy E^{opt} and exit.

In the initialization process, the reference energy E_{ref} in Step 2 on a Hartree-Fock state can be classically calculated efficiently. The energy E_i is measured on a quantum computer, which is the additional measurement cost compared to conventional VQE. In this work, we

use the first-order Trotter decomposition. Note that extra fine-tuning can be performed after step 3 by iteratively adding more operators to the ansatz until the energy difference $E^{(k-1)} - E^{(k)}$ between the $(k-1)$th and the kth iteration ($k \geq 1$) is smaller than a certain convergence criterion. In this work we skip this step for simplicity.

F. Computation of expectation value

The expectation will be calculated in a so-called democratic way, first proposed in Ref. [1]. It means if an operator has the indices from different fragments, the expectation of this operator will be the average of expectation for this operator in different fragments. For instance:

$$\langle \hat{a}_i^\dagger \hat{a}_j + \hat{a}_j^\dagger \hat{a}_i \rangle = \langle \Psi_A | \hat{a}_i^\dagger \hat{a}_j | \Psi_A \rangle + \langle \Psi_B | \hat{a}_j^\dagger \hat{a}_i | \Psi_B \rangle, \tag{21}$$

where the i and j belong to the fragment A and B, respectively. So are the two-body terms and so on.

II. TYPICAL DECOMPOSITION OF UNITARY EVOLUTION

In our work, the embedded small system is solved with high-level quantum solver, particularly in this work is mainly ESVQE. The ESVQE is well described in I E. The single- and double-excitation operators $\hat{T}_{pr}$ and $\hat{T}_{pqrs}$ are utilized to construct the compact quantum circuit.

For example, the wavefunction $|\Psi\rangle$ of a embedded system can be ideally constructed from the UCCSD ansatz $|\Psi\rangle = e^{\sum_{i=1}^{N_{op}} \hat{T}_i - \hat{T}_i^\dagger} |\Psi_0\rangle$, where T_i, N_{op} represents the corresponding single- and double excitions operators and number of operators in the selected operator pools. we perform the Jordan-Wigner transformation to change from fermion space to qubit space to enable the quantum simulation. Generally, the directly unitary evolution is hard to implement. so first-order Trotterization is always employed, results in quantum circuit generated as the product of a series of time evolution of Pauli strings like $U(\vec{\theta}) = e^{i\theta_1 \hat{P}_1} e^{i\theta_2 \hat{P}_2} e^{i\theta_3 \hat{P}_3} ...$, where $\hat{P}_i$ are Pauli strings.

Specially, for single excitation operators associate with coefficient θ that after Jordan-

Wigner transform, it can be written as [8]

$$\begin{aligned}\hat{t}_i^a - \hat{t}_i^{a\dagger} &= \theta(a_a^\dagger a_i - a_i^\dagger a_a) \\ &\overset{JW}{=} i\frac{\theta}{2}(\sigma_a^y\sigma_i^x - \sigma_a^x\sigma_i^y)\left(\bigotimes_{k=i+1}^{a-1}\sigma_k^z\right)\end{aligned} \tag{22}$$

$[\sigma_a^y\sigma_i^x, \sigma_m^x\sigma_n^y] = 0$ if $m \neq a, n \neq i$. Thus, after first-order Trotterization, the corresponding unitary operators may split as the product a series of unitary operator $e^{i\frac{\theta}{2}\sigma_a^y\sigma_k^z\cdots\sigma_i^x}, e^{i\frac{\theta}{2}\sigma_a^x\sigma_k^z\cdots\sigma_i^y}$, etc. Similarly, for the double excitation operators associated with another coefficient θ may leads to

$$\begin{aligned}\hat{t}_{ij}^{ab} - \hat{t}_{ij}^{ab\dagger} &= \theta(a_a^\dagger a_b^\dagger a_i a_j - a_j^\dagger a_i^\dagger a_b a_a) \\ &\overset{JW}{=} \frac{\theta}{8}(i\sigma_a^y\sigma_b^x\sigma_i^x\sigma_j^x - i\sigma_a^x\sigma_b^y\sigma_i^x\sigma_j^x - i\sigma_a^x\sigma_b^x\sigma_i^y\sigma_j^x \\ &+ i\sigma_a^x\sigma_b^x\sigma_i^x\sigma_j^y - i\sigma_a^y\sigma_b^y\sigma_i^y\sigma_j^x + i\sigma_a^y\sigma_b^y\sigma_i^x\sigma_j^y \\ &+ i\sigma_a^y\sigma_b^x\sigma_i^y\sigma_j^y - i\sigma_a^x\sigma_b^y\sigma_i^y\sigma_j^y)\left(\bigotimes_{k=m+1}^{i-1}\sigma_k^z\right)\left(\bigotimes_{p=n+1}^{j-1}\sigma_p^z\right),\end{aligned} \tag{23}$$

and it can be split as product of similar time evolution of single Pauli strings after Trotterization. To realize the time evolution of single Pauli strings, such as a typical operator $e^{i\theta\sigma_1^z\sigma_2^z\sigma_3^z\sigma_4^z}$ it may be decomposed into single-qubit rotation gates and two-qubit CNOT gate [9] as

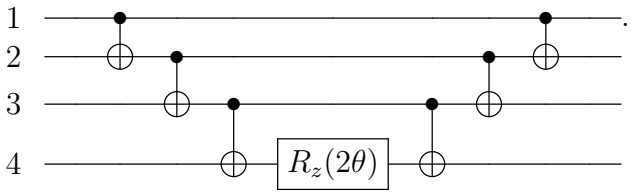

(24)

Other operators may be decomposed to similar circuits other than some different in single rotations. Generally, a time evolution of single Pauli string with length m (Note ignore the identity operator), assume n out of the m is Pauli Z operator, and the rest is either Pauli X or Y, then the corresponding gate number would be $2(m-1)$(CNOT gates) and $1+2(m-n)$(single-qubit gates) and the corresponding gate-depth would be $2(m-1)+1$ when $(m \neq n)$ or $2(m-1)+3$ when $(m \neq n)$. Note the above analysis does not take any hardware constraint into consideration, such as only allow nearest two-qubit gate and we also assume the basis-rotation single qubit gate can be implemented in parallel, so that 2 more extra depth is required when $m \neq n$.

According to ESVQE, each operators corresponding to one parameter. The operator did not selected into the operator pools shall disapper in $e^{\hat{t}-\hat{t}^\dagger}$ will be eliminated and the

corresponding Pauli strings in the quantum circuit shall disappear, leading to significant reduction to the circuit depth.

III. NUMERICAL RESULTS

A. Convergence of the DMET algorithm

In our simulation the DMET cost function $\mathcal{L}(\mu_{\text{global}})$ typically converges within a few round of iterations. In Table I, we display the convergence of the DMET cost functions in DMET iterations using different basis sets of the H_{10} system. Each DMET iteration corresponds to a certain number of ESVQE runs, depending on the fragmentation of the system. It is found that, regardless of the basis set used, the convergence of the cost function is reached within 3 to 4 iterations. Here the convergence threshold is set as 1×10^{-5}.

TABLE I. Convergence of the DMET cost function $\mathcal{L}(\mu_{\text{global}})$ in DMET iteration for the H_{10} system.

Basis Set	STO-3G			6-31G		
Bond Distance	1.0	2.0	2.8	1.0	2.0	2.8
Iteration 1	-2.2×10^{-3}	1.3×10^{-3}	6.2×10^{-5}	1.1×10^{-2}	4.4×10^{-2}	6.1×10^{-2}
Iteration 2	-1.3×10^{-3}	2.1×10^{-3}	2.8×10^{-4}	1.2×10^{-2}	4.6×10^{-2}	6.1×10^{-2}
Iteration 3	9.2×10^{-9}	-4.2×10^{-5}	3.0×10^{-9}	-2.2×10^{-5}	1.9×10^{-3}	-5.3×10^{-5}
Iteration 4	—	—	—	—	-2.7×10^{-5}	—

B. Absolute energies

In Table II, we list the absolute HF (either restricted or unrestricted), B3LYP, CCSD and DMET-ESVQE energies for the specified geometries of C_6H_8 hydrogenation and the C_{18} molecule. All methods except HF are non-variational, so direct comparisons of the absolute energies are of limited indication.

TABLE II. Absolute energies of the specified geometries of the systems invested in the main text by HF, B3LYP, CCSD and DMET-ESVQE. The meanings of the "Symbol"s can be found in the corresponding main text.

System	Basis	Symbol	HF	B3LYP	CCSD	DMET-ESVQE
C_6H_8+H_2	STO-3G	E_{TS}	-229.853	-231.361	-230.371	-230.275
C_{18}	STO-3G	E_{cumu}	-672.783	-676.324	-673.799	-674.325
C_{18}	cc-pVDZ	E_{cumu}	-681.204	-684.962	-683.223	-682.624

C. Analysis of the errors

Here we discuss the errors for DMET-ESVQE simulation in length to gain more insight into ESVQE and DMET. In Fig. 1 we show the relative error for the results derived by CCSD, ESVQE and DMET-ESVQE in the H_{10} system with STO-3G and 6-31G basis set. The reference ground truth is the results given by FCI in the respective basis set. In both panel (a) and panel (b) the convergence failure for CCSD is clearly visible. For STO-3G basis set, the results for conventional ESVQE is worse than DMET-ESVQE proposed here. This outcome might be surprising in the sense that the simulation of conventional ESVQE requires more qubits than DMET-ESVQE. Indeed, in the case where FCI is used as the high-level solver (DMET-FCI), DMET-FCI is apparently an approximation to the original FCI method and the role of DMET is to reduce the computational cost. The accuracy of DMET-FCI can be improved by using larger fragment size until the fragment size is equal to half of the whole system. However, the situation is not the same if approximate quantum chemistry solvers such as CCSD and ESVQE are considered. In the specific case of H_{10} with each single H atom as a fragment, it is well established that DMET-FCI produces the exact result in the dissociation limit [1]. The result is natural to understand in that DMET effectively adds up energies of individual H atoms which are treated at the FCI level. The key point of the H_{10} case is that DMET-CCSD or DMET-ESVQE is equivalent to DMET-FCI because the fragment+bath problem is a two-electron two-orbital problem. As a result, DMET-CCSD or DMET-ESVQE becomes more accurate than CCSD or ESVQE respectively at the dissociation limit. Despite the argument here, we do not anticipate that the DMET framework is able to reduce computational cost and improve accuracy

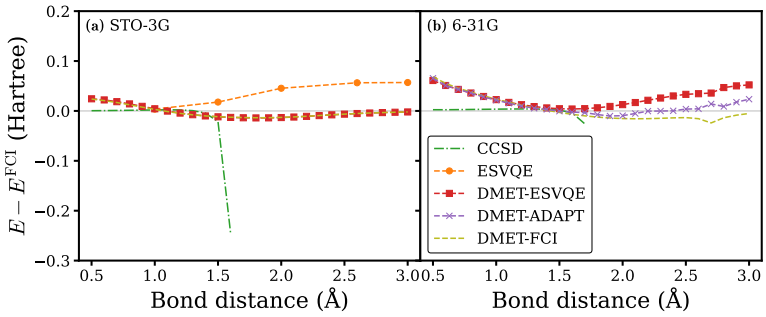

FIG. 1. Relative error for the homogeneous stretching of a evenly-spaced hydrogen chain composed of 10 atoms in (a) STO-3G and (b) 6-31G basis set.

simultaneously for general chemical systems. For 6-31G basis set, the error of DMET-ESVQE deviates from the error of DMET-FCI at the dissociation limit, which might be due to the energy sorting truncation of the ESVQE ansatz and the Trotter error [10]. Using more expensive VQE solver such as ADAPT-VQE [11] is possible to alleviate the problem. We term this approach as DMET-ADAPT. The implementation we use for ADAPT-VQE is Qiskit [12] (qiskit_nature version: 0.3.2) with default parameters, which means that the energy convergence threshold is set to 1×10^{-5}. It is shown in Fig. 1 that, as a more expensive method, DMET-ADAPT yields more accurate results than DMET-ESVQE. However, the simulation is much more time consuming, and the error at long bond distance compared to DMET-FCI is still visible.

The potential energy curves by CCSD and DMET-ESVQE shown in the main text are not well aligned. In Fig. 2 we explore its origin by checking the convergence of fragment size with STO-3G basis set using CCSD as the high-level solver, termed as DMET-CCSD. Here we have replaced ESVQE with CCSD because their performance should be of the same level. The fragment size is defined as the number of carbon atoms contained in each fragment. For the $\theta = 16°$ geometry and the $\theta = 18°$ geometry we find that by increasing the fragment size the energy obtained by DMET-CCSD converges to the energy obtained by CCSD and $E - E^{\mathrm{CCSD}}$ approaches to zero. When the number of carbon atoms in the fragment is 9, DMET-CCSD effectively reduces to CCSD. For the $\theta = 20°$ geometry, the difference between DMET-CCSD and CCSD abruptly increases when there are 3 carbon atoms in each fragment. This is actually a known issue of DMET that using larger fragment size might deteriorate the outcome [1] and strategies to improve this shortcoming are under

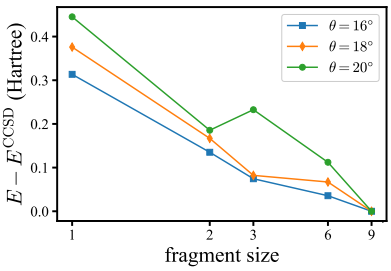

FIG. 2. The convergence of DMET with respect to the fragment size using CCSD as the high level solver. The reference energy E^{CCSD} is obtained by solving the whole C_{18} molecule using CCSD. The fragment size is defined as the number of carbon atoms in each fragment.

active development [13–15]. In principle, using a larger fragment size produces more accurate DMET energy. However, such a tendency may suffer from different issues. The DMET method itself is not variational and the fragment size is not identical to the size of active space in CI methods. Besides, increasing the DMET fragment size has a side effect that may increase the error of the high-level solver. When a larger DMET fragment size is used, the embedded problem becomes more complex and the high-level solver might be less efficient and hence become more inaccurate, leading to deteriorated results. This effect is manifested in Fig. 1 of the supporting information and is discussed in detail.

[1] S. Wouters, C. A. Jiménez-Hoyos, Q. Sun, and G. K.-L. Chan, A practical guide to density matrix embedding theory in quantum chemistry, J. Chem. Theory Comput. **12**, 2706 (2016).

[2] G. Knizia and G. K.-L. Chan, Density matrix embedding: A simple alternative to dynamical mean-field theory, Phys. Rev. Lett. **109**, 186404 (2012).

[3] G. Knizia and G. K.-L. Chan, Density matrix embedding: A strong-coupling quantum embedding theory, J. Chem. Theory Comput. **9**, 1428 (2013).

[4] Q. Sun and G. K.-L. Chan, Exact and optimal quantum mechanics/molecular mechanics boundaries, J. Chem. Theory Comput. **10**, 3784 (2014).

[5] Q. Sun, X. Zhang, S. Banerjee, P. Bao, M. Barbry, N. S. Blunt, N. A. Bogdanov, G. H. Booth, J. Chen, Z.-H. Cui, J. J. Eriksen, Y. Gao, S. Guo, J. Hermann, M. R. Hermes, K. Koh, P. Koval, S. Lehtola, Z. Li, J. Liu, N. Mardirossian, J. D. McClain, M. Motta, B. Mussard, H. Q. Pham, A. Pulkin, W. Purwanto, P. J. Robinson, E. Ronca, E. R. Sayfutyarova, M. Scheurer,

H. F. Schurkus, J. E. T. Smith, C. Sun, S.-N. Sun, S. Upadhyay, L. K. Wagner, X. Wang, A. White, J. D. Whitfield, M. J. Williamson, S. Wouters, J. Yang, J. M. Yu, T. Zhu, T. C. Berkelbach, S. Sharma, A. Y. Sokolov, and G. K.-L. Chan, Recent developments in the PySCF program package, J. Chem. Phys. **153**, 024109 (2020).

[6] G. Knizia, Intrinsic atomic orbitals: An unbiased bridge between quantum theory and chemical concepts, J. Chem. Theory Comput. **9**, 4834 (2013).

[7] J. K. L. MacDonald, Successive approximations by the Rayleigh-Ritz variation method, Phys. Rev. **43**, 830 (1933).

[8] C. Cao, J. Hu, W. Zhang, X. Xu, D. Chen, F. Yu, J. Li, H. Hu, D. Lv, and M.-H. Yung, Towards a larger molecular simulation on the quantum computer: Up to 28 qubits systems accelerated by point group symmetry, arXiv preprint arXiv:2109.02110 (2021).

[9] M. A. Nielsen and I. Chuang, Quantum computation and quantum information, American Journal of Physics **70**, 558 (2002).

[10] H. R. Grimsley, D. Claudino, S. E. Economou, E. Barnes, and N. J. Mayhall, Is the Trotterized uccsd ansatz chemically well-defined?, J. Chem. Theory Comput. **16**, 1 (2020).

[11] H. R. Grimsley, S. E. Economou, E. Barnes, and N. J. Mayhall, An adaptive variational algorithm for exact molecular simulations on a quantum computer, Nat. Commun. **10**, 3007 (2019).

[12] M. S. ANIS, Abby-Mitchell, H. Abraham, AduOffei, R. Agarwal, G. Agliardi, M. Aharoni, I. Y. Akhalwaya, G. Aleksandrowicz, T. Alexander, M. Amy, S. Anagolum, Anthony-Gandon, E. Arbel, A. Asfaw, A. Athalye, A. Avkhadiev, C. Azaustre, P. BHOLE, A. Banerjee, S. Banerjee, W. Bang, A. Bansal, P. Barkoutsos, A. Barnawal, G. Barron, G. S. Barron, L. Bello, Y. Ben-Haim, M. C. Bennett, D. Bevenius, D. Bhatnagar, A. Bhobe, P. Bianchini, L. S. Bishop, C. Blank, S. Bolos, S. Bopardikar, S. Bosch, S. Brandhofer, Brandon, S. Bravyi, N. Bronn, Bryce-Fuller, D. Bucher, A. Burov, F. Cabrera, P. Calpin, L. Capelluto, J. Carballo, G. Carrascal, A. Carriker, I. Carvalho, A. Chen, C.-F. Chen, E. Chen, J. C. Chen, R. Chen, F. Chevallier, K. Chinda, R. Cholarajan, J. M. Chow, S. Churchill, CisterMoke, C. Claus, C. Clauss, C. Clothier, R. Cocking, R. Cocuzzo, J. Connor, F. Correa, Z. Crockett, A. J. Cross, A. W. Cross, S. Cross, J. Cruz-Benito, C. Culver, A. D. Córcoles-Gonzales, N. D, S. Dague, T. E. Dandachi, A. N. Dangwal, J. Daniel, M. Daniels, M. Dartiailh, A. R. Davila, F. Debouni, A. Dekusar, A. Deshmukh, M. Deshpande, D. Ding, J. Doi, E. M. Dow,

E. Drechsler, E. Dumitrescu, K. Dumon, I. Duran, K. EL-Safty, E. Eastman, G. Eberle, A. Ebrahimi, P. Eendebak, D. Egger, ElePT, Emilio, A. Espiricueta, M. Everitt, D. Facoetti, Farida, P. M. Fernández, S. Ferracin, D. Ferrari, A. H. Ferrera, R. Fouilland, A. Frisch, A. Fuhrer, B. Fuller, M. GEORGE, J. Gacon, B. G. Gago, C. Gambella, J. M. Gambetta, A. Gammanpila, L. Garcia, T. Garg, S. Garion, J. R. Garrison, J. Garrison, T. Gates, L. Gil, A. Gilliam, A. Giridharan, J. Gomez-Mosquera, Gonzalo, S. de la Puente González, J. Gorzinski, I. Gould, D. Greenberg, D. Grinko, W. Guan, D. Guijo, J. A. Gunnels, H. Gupta, N. Gupta, J. M. Günther, M. Haglund, I. Haide, I. Hamamura, O. C. Hamido, F. Harkins, K. Hartman, A. Hasan, V. Havlicek, J. Hellmers, Ł. Herok, S. Hillmich, H. Horii, C. Howington, S. Hu, W. Hu, J. Huang, R. Huisman, H. Imai, T. Imamichi, K. Ishizaki, Ishwor, R. Iten, T. Itoko, A. Ivrii, A. Javadi, A. Javadi-Abhari, W. Javed, Q. Jianhua, M. Jivrajani, K. Johns, S. Johnstun, Jonathan-Shoemaker, JosDenmark, JoshDumo, J. Judge, T. Kachmann, A. Kale, N. Kanazawa, J. Kane, Kang-Bae, A. Kapila, A. Karazeev, P. Kassebaum, T. Kehrer, J. Kelso, S. Kelso, V. Khanderao, S. King, Y. Kobayashi, Kovi11Day, A. Kovyrshin, R. Krishnakumar, V. Krishnan, K. Krsulich, P. Kumkar, G. Kus, R. LaRose, E. Lacal, R. Lambert, H. Landa, J. Lapeyre, J. Latone, S. Lawrence, C. Lee, G. Li, J. Lishman, D. Liu, P. Liu, Lolcroc, A. K. M, L. Madden, Y. Maeng, S. Maheshkar, K. Majmudar, A. Malyshev, M. E. Mandouh, J. Manela, Manjula, J. Marecek, M. Marques, K. Marwaha, D. Maslov, P. Maszota, D. Mathews, A. Matsuo, F. Mazhandu, D. McClure, M. McElaney, C. McGarry, D. McKay, D. McPherson, S. Meesala, D. Meirom, C. Mendell, T. Metcalfe, M. Mevissen, A. Meyer, A. Mezzacapo, R. Midha, D. Miller, Z. Minev, A. Mitchell, N. Moll, A. Montanez, G. Monteiro, M. D. Mooring, R. Morales, N. Moran, D. Morcuende, S. Mostafa, M. Motta, R. Moyard, P. Murali, J. Müggenburg, T. NEMOZ, D. Nadlinger, K. Nakanishi, G. Nannicini, P. Nation, E. Navarro, Y. Naveh, S. W. Neagle, P. Neuweiler, A. Ngoueya, T. Nguyen, J. Nicander, Nick-Singstock, P. Niroula, H. Norlen, NuoWenLei, L. J. O'Riordan, O. Ogunbayo, P. Ollitrault, T. Onodera, R. Otaolea, S. Oud, D. Padilha, H. Paik, S. Pal, Y. Pang, A. Panigrahi, V. R. Pascuzzi, S. Perriello, E. Peterson, A. Phan, K. Pilch, F. Piro, M. Pistoia, C. Piveteau, J. Plewa, P. Pocreau, A. Pozas-Kerstjens, R. Pracht, M. Prokop, V. Prutyanov, S. Puri, D. Puzzuoli, J. Pérez, Quant02, Quintiii, R. I. Rahman, A. Raja, R. Rajeev, I. Rajput, N. Ramagiri, A. Rao, R. Raymond, O. Reardon-Smith, R. M.-C. Redondo, M. Reuter, J. Rice, M. Riedemann, Rietesh, D. Risinger, M. L. Rocca, D. M. Rodríguez, RohithKarur, B. Rosand,

M. Rossmannek, M. Ryu, T. SAPV, N. R. C. Sa, A. Saha, A. Ash-Saki, S. Sanand, M. Sandberg, H. Sandesara, R. Sapra, H. Sargsyan, A. Sarkar, N. Sathaye, B. Schmitt, C. Schnabel, Z. Schoenfeld, T. L. Scholten, E. Schoute, M. Schulterbrandt, J. Schwarm, J. Seaward, Sergi, I. F. Sertage, K. Setia, F. Shah, N. Shammah, R. Sharma, Y. Shi, J. Shoemaker, A. Silva, A. Simonetto, D. Singh, D. Singh, P. Singh, P. Singkanipa, Y. Siraichi, Siri, J. Sistos, I. Sitdikov, S. Sivarajah, M. B. Sletfjerding, J. A. Smolin, M. Soeken, I. O. Sokolov, I. Sokolov, V. P. Soloviev, SooluThomas, Starfish, D. Steenken, M. Stypulkoski, A. Suau, S. Sun, K. J. Sung, M. Suwama, O. Słowik, H. Takahashi, T. Takawale, I. Tavernelli, C. Taylor, P. Taylour, S. Thomas, K. Tian, M. Tillet, M. Tod, M. Tomasik, C. Tornow, E. de la Torre, J. L. S. Toural, K. Trabing, M. Treinish, D. Trenev, TrishaPe, F. Truger, G. Tsilimigkounakis, D. Tulsi, W. Turner, Y. Vaknin, C. R. Valcarce, F. Varchon, A. Vartak, A. C. Vazquez, P. Vijaywargiya, V. Villar, B. Vishnu, D. Vogt-Lee, C. Vuillot, J. Weaver, J. Weidenfeller, R. Wieczorek, J. A. Wildstrom, J. Wilson, E. Winston, WinterSoldier, J. J. Woehr, S. Woerner, R. Woo, C. J. Wood, R. Wood, S. Wood, J. Wootton, M. Wright, L. Xing, J. YU, B. Yang, U. Yang, J. Yao, D. Yeralin, R. Yonekura, D. Yonge-Mallo, R. Yoshida, R. Young, J. Yu, L. Yu, C. Zachow, L. Zdanski, H. Zhang, I. Zidaru, C. Zoufal, aeddins ibm, alexzhang13, b63, bartek bartlomiej, bcamorrison, brandhsn, charmerDark, deeplokhande, dekel.meirom, dime10, dlasecki, ehchen, fanizzamarco, fs1132429, gadial, galeinston, georgezhou20, georgios ts, gruu, hhorii, hykavitha, itoko, jeppevinkel, jessica angel7, jezerjojo14, jliu45, jscott2, klinvill, krutik2966, ma5x, michelle4654, msuwama, nico lgrs, ntgiwsvp, ordmoj, sagar pahwa, pritamsinha2304, ryancocuzzo, saktar unr, saswati qiskit, septembrr, sethmerkel, sg495, shaashwat, smturro2, sternparky, strickroman, tigerjack, tsura crisaldo, upsideon, vadebayo49, welien, willhbang, wmurphy collabstar, yang.luh, and M. Čepulkovskis, Qiskit: An open-source framework for quantum computing (2021).

[13] M. Welborn, T. Tsuchimochi, and T. Van Voorhis, Bootstrap embedding: An internally consistent fragment-based method, J. Chem. Phys. **145**, 074102 (2016).

[14] H.-Z. Ye, N. D. Ricke, H. K. Tran, and T. Van Voorhis, Bootstrap embedding for molecules, J. Chem. Theory Comput. **15**, 4497 (2019).

[15] H.-Z. Ye, H. K. Tran, and T. Van Voorhis, Bootstrap embedding for large molecular systems, J. Chem. Theory Comput. **16**, 5035 (2020).